

## Structural change of ion-induced carbon nanofibers by electron current flow

Mohd Zamri, Pradip Ghosh, Akari Hayashi, Yasuhiko Hayashi, Masaki Tanemura et al.

Citation: *J. Vac. Sci. Technol. B* **29**, 04E103 (2011); doi: 10.1116/1.3591420

View online: <http://dx.doi.org/10.1116/1.3591420>

View Table of Contents: <http://avspublications.org/resource/1/JVTBD9/v29/i4>

Published by the AVS: Science & Technology of Materials, Interfaces, and Processing

### Related Articles

Growth characterization of electron-beam-induced silver deposition from liquid precursor  
*J. Vac. Sci. Technol. B* **30**, 06FF08 (2012)

Stabilization of field electron emission from carbon nanofibers using ballast resistance  
*J. Vac. Sci. Technol. B* **30**, 031801 (2012)

LaMnO<sub>3</sub>: Influence of the Addition of Ba and Sr  
*Surf. Sci. Spectra* **16**, 83 (2009)

Cu<sub>x</sub>O - TiO<sub>2</sub> Composites (x=1, 2) Studied by X-ray Photoelectron Spectroscopy  
*Surf. Sci. Spectra* **16**, 1 (2009)

Embedded ErAs nanorods on GaAs (n11) substrates by molecular beam epitaxy  
*J. Vac. Sci. Technol. B* **29**, 03C108 (2011)

### Additional information on *J. Vac. Sci. Technol. B*

Journal Homepage: <http://avspublications.org/jvstb>

Journal Information: [http://avspublications.org/jvstb/about/about\\_the\\_journal](http://avspublications.org/jvstb/about/about_the_journal)

Top downloads: [http://avspublications.org/jvstb/top\\_20\\_most\\_downloaded](http://avspublications.org/jvstb/top_20_most_downloaded)

Information for Authors: [http://avspublications.org/jvstb/authors/information\\_for\\_contributors](http://avspublications.org/jvstb/authors/information_for_contributors)

## ADVERTISEMENT

# Instruments for advanced science

**Gas Analysis**



- dynamic measurement of reaction gas streams
- catalysis and thermal analysis
- molecular beam studies
- dissolved species probes
- fermentation, environmental and ecological studies

**Surface Science**



- UHV TPD
- SIMS
- end point detection in ion beam etch
- elemental imaging - surface mapping

**Plasma Diagnostics**



- plasma source characterization
- etch and deposition process reaction kinetic studies
- analysis of neutral and radical species

**Vacuum Analysis**



- partial pressure measurement and control of process gases
- reactive sputter process control
- vacuum diagnostics
- vacuum coating process monitoring

contact Hiden Analytical for further details

**HIDEN ANALYTICAL**

[info@hideninc.com](mailto:info@hideninc.com)  
[www.HidenAnalytical.com](http://www.HidenAnalytical.com)

CLICK to view our product catalogue 

# Structural change of ion-induced carbon nanofibers by electron current flow

Mohd Zamri<sup>a)</sup>

Department of Frontier Materials, Nagoya Institute of Technology, Gokiso-cho, Showa-ku, 466-8555 Nagoya, Japan and Department of Materials, Faculty of Mechanical Engineering, Universiti Teknologi Malaysia, 81310 UTM Skudai, Johor, Malaysia

Pradip Ghosh, Akari Hayashi, Yasuhiko Hayashi, and Masaki Tanemura

Department of Frontier Materials, Nagoya Institute of Technology, Gokiso-cho, Showa-ku, 466-8555, Nagoya, Japan

Masato Sasase

Wakasawan Energy Research Center, Nagayoshi-cho 64-52-1, Tsuruga-shi, 914-0192 Fukui, Japan

(Received 15 November 2010; accepted 23 April 2011; published 14 June 2011)

A graphite foil was irradiated with argon ( $\text{Ar}^+$ ) ions to fabricate conical structures with a carbon nanofiber (CNF) on top of the structure. The field emission (FE) properties of one-dimensional individual CNF-tipped cones that had been fabricated were carefully measured by *in situ* transmission electron microscopy (TEM) facilities. The highest FE current, 550 nA, was observed in the current-voltage (I-V) measurement of a single CNF. Almost no degradation in I-V properties were detected during the reliability test after 30 min. TEM images indicated that the CNF was amorphous in nature initially, and that the electron current flow in the FE process induced the dramatic change in the crystalline structure of both the CNF and of the tip region of the basal cone part. After performing the FE process, the crystalline structures of the amorphous CNFs were transformed into ring-shaped graphene layers, whereas nanodiamond like nanoparticles formed in the outer layer of the tip region of the basal cone. The structural changes induced can be attributed to Joule heating under the high electric field. © 2011 American Vacuum Society.

[DOI: 10.1116/1.3591420]

## I. INTRODUCTION

With the continuing enormous interest in the development of field emission (FE) sources, many works over the past few years have been devoted to verifying the performance of the nanomaterial as the source of electron emitters.<sup>1-3</sup> Thus, emission stability,<sup>4,5</sup> low turn-on field,<sup>6</sup> material reliability,<sup>4,7,8</sup> and materials implementation to the production field<sup>9,10</sup> have been investigated deeply. Some of the best electron emitters are one-dimensional (1-D) carbon nanomaterials such as carbon nanotubes (CNTs) and carbon nanofibers (CNFs).<sup>11</sup> The advantages of CNTs and CNFs are that they feature a quite high aspect ratio as well as a sharp tip radius, leading to a restraint in the applied voltage to emit electrons even at low vacuum pressure.

In our previous works, we demonstrated that  $\text{Ar}^+$  ion irradiation onto the carbon surfaces (both bulk and carbon coating) induced the formation of conical structures. We also demonstrated that the CNFs grew on the top of the structures even at room temperature without any catalyst.<sup>11</sup> The FE properties (initial property and emission stability) of the ion-induced CNFs are comparable with that of CNTs grown by a high temperature process such as plasma-enhanced chemical vapor deposition method.<sup>9,10</sup> Ion-induced CNFs are amorphous in crystalline nature.<sup>4</sup> We seek to answer the question:

Does the structure still remain amorphous in character after completing the stability test in FE measurement? For the practical use of ion-induced CNFs, it is highly essential to understand fully the fundamental physics underlying the FE process for individual CNF emitters.

In this work, ion-induced CNFs that were fabricated at room temperature were chosen as the emitter. We investigated the CNFs' structural change through electron current flow during the FE process, using *in situ* transmission electron microscopy (TEM) facilities. The FE properties and the current stability for the single CNF were also carefully measured.

## II. EXPERIMENTAL METHODS

We used a Kaufmann-type ion gun (Iontech, Inc. Ltd., model 3-1500-100FC) for fabricating the CNFs. The samples we used were commercially available graphite foils of dimensions  $5 \times 10 \times 100 \mu\text{m}$ . The edges of the foils were irradiated with  $\text{Ar}^+$  ions, as explained below. The growth mechanism of ion-induced CNFs is explained elsewhere in detail.<sup>11</sup> In brief, sputter-ejected carbon atoms from the carbon surface were redeposited onto the sidewall of the ion-induced conical surface protrusions. Next, the redeposited carbon atoms diffused toward the cone tip to form the CNFs without any catalyst even at room temperature. For the controlled CNF growth, the carbon supply played an important role. For this part, an additional carbon plate of dimensions

<sup>a)</sup>Author to whom correspondence should be addressed; electronic mail: zamriusop@fkm.utm.my

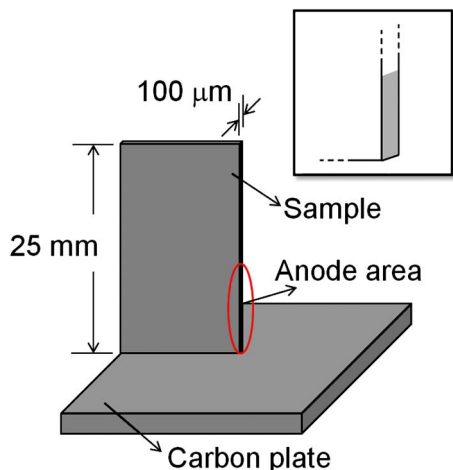


FIG. 1. (Color online) Sample setup for fabricating CNFs. The inset shows the marked area where CNFs were mostly grown.

$10 \times 10 \times 2$  mm was horizontally placed adjacent to the graphite foil. Next, they were coirradiated with  $\text{Ar}^+$  ions at an incidence angle of  $45^\circ$  from the normal to the surface for 45 min (Fig. 1). The oblique  $\text{Ar}^+$  ion bombardment was found to be more suitable for the growth of ion-induced CNFs than normal incidence.<sup>12,13</sup> The diameter and ion beam energy employed for this experiment were 6 cm and 1 keV, respectively. The basal and working pressures were  $1.5 \times 10^{-5}$  and  $2.0 \times 10^{-2}$  Pa, respectively.

After sputtering, the morphology of the CNFs grown at the edge of the graphite foil was carefully observed using a scanning electron microscope [SEM (JEOL JSM-5600)]. In addition, the crystallinity of the sample was examined by TEM (JEOL JEM-3010). We used a TEM sample holder (JEOL; EM-Z02154T) with a piezo-controlled tungsten (W) nanoprobe coated with gold (Au) to measure the current-voltage (I-V) characteristics of the single CNF sample. The graphite foil was cut into small square pieces of 2 mm side length and directly mounted on the TEM sample holder without any other post treatment.

### III. RESULTS AND DISCUSSION

Figures 2(a) and 2(b) show the SEM images of the graphite foils' edge surfaces after the  $\text{Ar}^+$  ion irradiation. It should be noted that for the ion irradiation method, only a CNF grew on the respective cones and no CNF grew without any cone bases. In the present experiment, the carbon supply rate from the carbon plate was dependent upon the distance from the carbon plate; the carbon supply rate was highest at the base of the graphite foil and decreased gradually toward the top. As seen in Figs. 2(a) and 2(b), the morphological structure of CNFs varies depending on the distance from the carbon plate. The surface of the base was covered with densely distributed cones, while single CNFs grew on the respective cone tops [Fig. 2(b)]. The CNFs were small, 20–50 nm in diameter, and  $0.5$ – $2$   $\mu\text{m}$  in length [Fig. 2(b) inset]. In contrast, the surface of the top of the graphite foil was covered by relatively large cones, some of which possessed the single

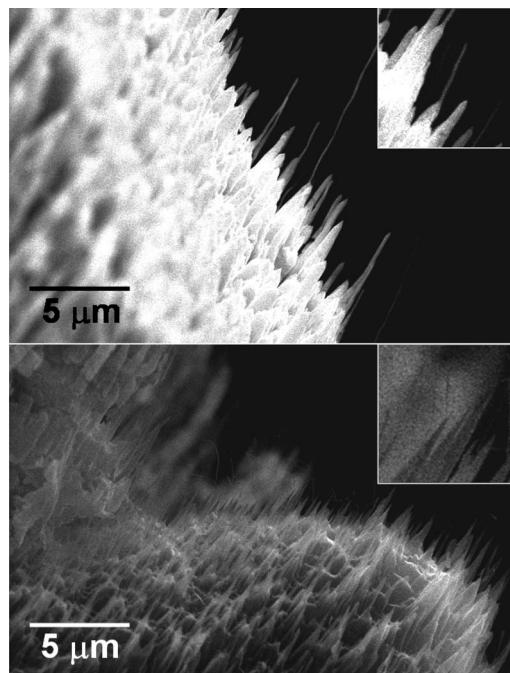


FIG. 2. (a) SEM image of the morphology of CNFs at the top area of the graphite edge after  $\text{Ar}^+$  ion bombardment and (b) SEM image of the morphology of CNFs at the bottom area of the graphite edge after  $\text{Ar}^+$  ion bombardment.

CNFs on top [Fig. 2(a)]. In this case, the CNFs were found to be relatively larger: 100–200 nm in diameter, and 1.0–5.0  $\mu\text{m}$  in length [Inset of Fig. 2(a)]. For the measurement of the FE properties of individual CNFs in the TEM system, we used the smaller CNFs formed at the bottom area of the graphite foil's edge. In order to avoid the interference of the adjacent CNFs during the I-V measurement of the individual CNF, surrounding CNFs were carefully removed with an anode nanoprobe (Au coated W) while monitoring TEM images of the CNF and the anode before I-V measurements.

Figure 3 shows the TEM images of a single CNF. The CNF was 660 nm in length and 20 nm in diameter. The inset shows a high resolution TEM image. The TEM image can be used to observe the detailed crystalline structure of the stem region of the CNF. High-resolution TEM images revealed that several small crystallites were dispersed in the amorphous matrix of the CNF. The other region of the CNF was found to be amorphous in nature.

To investigate the FE properties of this single CNF, we applied a voltage from 0 to 120 V at an incremental step of 10 V using a 50 k $\Omega$  resistor connected in a series while observing the crystalline structure at  $\times 30\,000$  magnification in TEM. The distance between the CNF tip and the Au coated W nanoprobe (anode) was 1.3  $\mu\text{m}$ . The pressure in the specimen chamber was about  $10^{-5}$  Pa during the measurement. The FE properties were measured four times. When the voltage was applied to the CNF, the structure of the CNF was bent toward the anode due to the applied electric field.

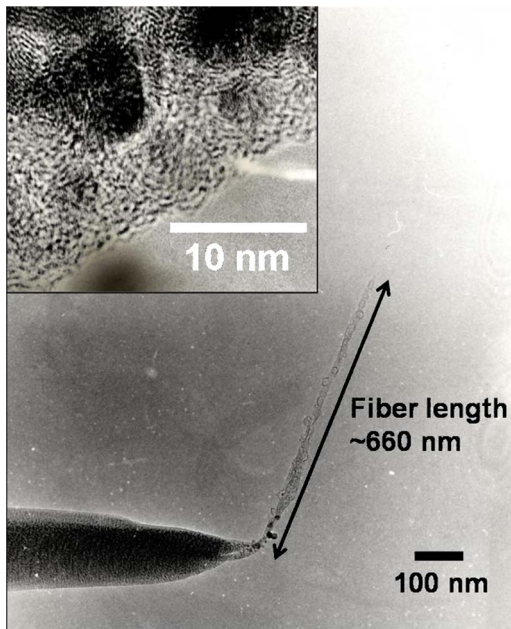


FIG. 3. (Color online) TEM image of the structure of CNF before the FE process. The inset shows the amorphous nature of the CNF at the stem part of it.

Figure 4(a) shows the FE properties of the single CNF. The highest emission current, 550 nA, was recorded on the fourth cycle with an applied voltage of 120 V. The turn-on fields corresponding to the current value of 1 nA were in the range of 70–80 V/ $\mu\text{m}$ . The threshold fields, which we defined here as the field required to achieve a current value of 100 nA, were in the range of 95–100 V/ $\mu\text{m}$ . After the FE measurements, we also tested the stability in emission current from the single CNF. The initial emission current was set at  $\sim 500$  nA with an applied voltage of 150 V. Figure 4(b) shows the result of the reliability test, disclosing that the emission current was maintained at around 500 nA without remarkable degradation for more than 30 min.

We investigated the structural and crystallinity changes of the single CNF after the FE measurements. Figure 5 shows a TEM image of the CNF with a high magnification image (inset) of the stem part of the CNF corresponding to the inset in Fig. 2 after the FE measurements. The fiber length was reduced from 660 to 350 nm after the FE measurements. In addition, from a comparison of Figs. 3 and 5, it is clear that the crystallinity of the CNF structure was significantly changed from amorphous and/or very fine crystallites (Fig. 3) to a graphitic structure (Fig. 5). As clearly seen in the inset of Fig. 5, the CNF consisted of ring-shaped stacked-graphene layers after the FE measurement.

Figures 6(a) and 6(b) show the enlarged TEM images of the tip region of the cone and the stem part of the CNF taken before and after the FE measurements, respectively. Before the FE measurement, the tip region of the cone consisted of very fine crystallites [Fig. 6(a)]. The selected area electron diffraction (SAED) pattern shows (010), (111), and (120) ring patterns of very fine graphitic polycrystalline structures. In contrast, after the FE measurements, many particles about

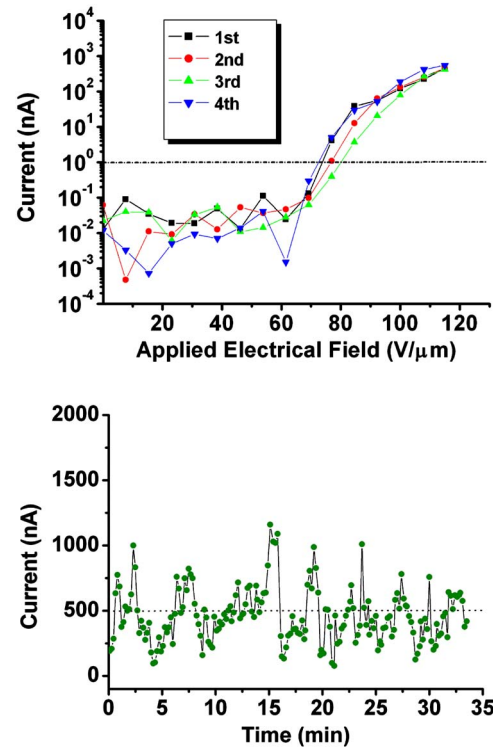


FIG. 4. (a) FE plot (Current (nA) vs Applied Electrical Field (V/ $\mu\text{m}$ )) of the CNF shown in Fig. 3. (b) The reliability test of the emission current for the CNF shown in Fig. 3. The initial current was fixed at  $\sim 500$  nA at an applied voltage of 150 V for more than 30 min.

10 nm in diameter were dispersed on the cone tip region. A high magnification TEM image verifies that these particles possessed polycrystalline structures with a lattice distance around 1.95 Å [Fig. 6(b) inset]. Further study of the SAED pattern shows that these polycrystalline structures were very close to that of diamond (111) (2.05 Å) lattice distance. What are the main mechanisms of the FE-induced structural change of CNFs? The most probable factor will be the Joule

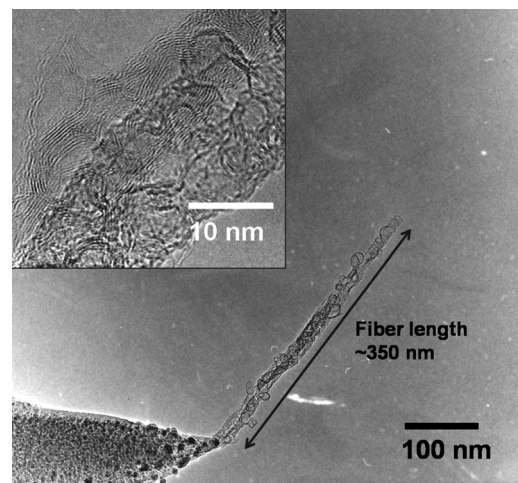


FIG. 5. TEM image of the CNF structure after the FE process. The inset shows the magnified TEM image of the CNF, indicating the formation of ring-like stacks of graphene layers.

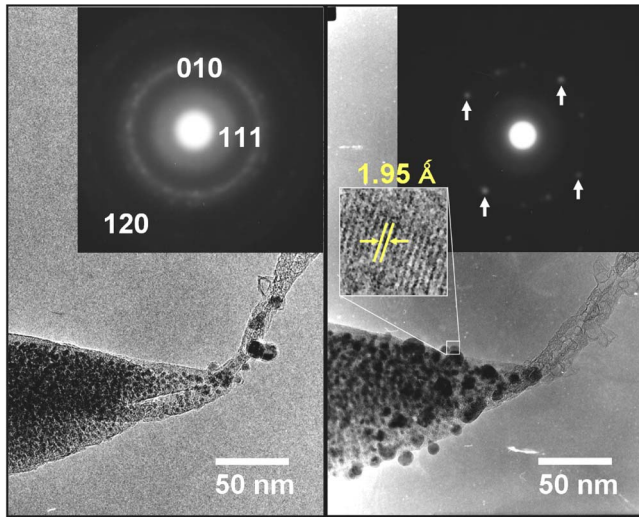


FIG. 6. (Color online) TEM images of the structure of the tip part of the cone taken (a) before and (b) after the FE process. Insets show the SAED patterns at the tip part of the cone taken (a) before and (b) after the FE process.

heating induced by the current flow. According to Vincent *et al.*, the temperature rise of 1-D objects during the FE process can be estimated using a resistive heating model.<sup>14</sup> For a 1-D object like a CNF, the temperature distribution equation is expressed as follows:

$$\Delta T(K) = T_L(K) - T_0(K) = \frac{RLI^2}{2\kappa A}, \quad (1)$$

where  $R$  is the resistivity of CNTs/CNFs ( $2.0 \times 10^6 \Omega$ ),  $\kappa$  is the thermal conductivity (100 W/mK),  $A = \pi r^2$ , the cross sectional area of a CNF, and  $I$  is the emission current. In our present experiment, the length and radius of the CNF were found to be 660 and  $\sim 10$  nm, respectively. If we consider the emitter length to be the distance from the cone base to the CNF tip, the total length was calculated to be  $1.66 \mu\text{m}$ . The emission current ranged from 450 to 1160 nA. The emission current would flow along the CNF through the outer surface and hence most of the structural change would occur from the outer layers.<sup>15</sup> If the outer layer thickness is assumed to be 0.34 nm (corresponding to the one layer thickness of graphene), the temperature of the outer layer during the FE process, estimated from the above Eq. (1), would reach 1350 K, which would be high enough for the recrystallization of the CNF structure. Next, the CNF was placed under a high electric field of  $115 \text{ V}/\mu\text{m}$ . Such a high electric field might induce an atomic arrangement more readily. Weakly bonded amorphous carbon would be field-evaporated, and thus only the graphitized carbon would remain. In fact, the reduction in CNF length is seen in the comparison between Figs. 3 and 5. Therefore, generation of Joule heating under the high electric field would be respon-

sible for the structural change of the CNFs. To confirm this, systematic investigations on structural change induced by current flow with and without high electric fields using various kinds of ion-induced carbon-based CNFs and various 1-D nanomaterials will be necessary. Experiments along this line are currently being undertaken and will be dealt with in our forthcoming paper.

#### IV. SUMMARY AND CONCLUSIONS

In summary, the FE-induced structural change of a CNF-tipped cone fabricated on the edge of a graphite foil was observed by *in situ* TEM analysis. The FE properties of the single CNF showed that the highest current was 550 nA. In the reliability test, the stable current flow of about 500 nA for more than 30 min was confirmed. After these FE measurements, the dramatic change in the crystalline structure from amorphous and/or very fine crystallites to graphitic structure was observed for both the CNF and the tip region of the basal cone. The amorphous CNF was transformed into ring-shaped graphene layers, whereas nanodiamond like nanoparticles were observed in the outer layer of the tip region of the basal cone. We predict that Joule heating under a high electric field could be responsible for the structural change of the CNFs.

#### ACKNOWLEDGMENT

This work was partially supported by the Grant of Wakasa-wan Energy Research Center.

- <sup>1</sup>E. Minoux *et al.*, *Nano Lett.* **5**, 2135 (2005).
- <sup>2</sup>H. He, Jr., R. Yang, Y. L. Chueh, L. J. Chou, L. J. Chen, and Z. L. Wang, *Adv. Mater.* (Weinheim, Ger.) **18**, 650 (2006).
- <sup>3</sup>N. Shang, P. Papakonstantinou, P. Wang, A. Zakharov, U. Palnitkar, N. Lin, M. Chu, and A. Stamboulis, *ACS Nano* **3**, 1032 (2009).
- <sup>4</sup>M. Tanemura *et al.*, *Appl. Phys. Lett.* **87**, 193102 (2005).
- <sup>5</sup>K. Uppireddi, B. Yang, P. X. Feng, and G. Morell, *Appl. Phys. Lett.* **95**, 242103 (2009).
- <sup>6</sup>Y. W. Zhu, H. Z. Zhang, X. C. Sun, S. Q. Feng, J. Xu, Q. Zhao, B. Xiang, R. M. Wang, and D. P. Yu, *Appl. Phys. Lett.* **83**, 144 (2003).
- <sup>7</sup>H. C. Lo, D. Das, J. S. Hwang, K. H. Chen, C. H. Hsu, C. F. Chen, and L. C. Chen, *Appl. Phys. Lett.* **83**, 1420 (2003).
- <sup>8</sup>N. G. Shang, P. Papakonstantinou, J. McLaughlin, W. C. Chen, L. C. Chen, M. Chu, and A. Stamboulis, *J. Appl. Phys.* **103**, 124308 (2008).
- <sup>9</sup>H. S. Sim, S. P. Lau, H. Y. Yang, L. K. Ang, M. Tanemura, and K. Yamaguchi, *Appl. Phys. Lett.* **90**, 143103 (2007).
- <sup>10</sup>S. Hofmann, C. Ducati, B. Kleinsorge, and J. Robertson, *Appl. Phys. Lett.* **83**, 4661 (2003).
- <sup>11</sup>M. Tanemura, T. Okita, H. Yamauchi, S. Tanemura, and R. Morishima, *Appl. Phys. Lett.* **84**, 3831 (2004).
- <sup>12</sup>M. Tanemura, T. Okita, J. Tanaka, H. Yamauchi, L. Miao, S. Tanemura, and R. Morishima, *Eur. Phys. J. D* **34**, 283 (2005).
- <sup>13</sup>M. Zamri, P. Ghosh, Z. P. Wang, M. Kawagishi, A. Hayashi, Y. Hayashi, and M. Tanemura, *J. Vac. Sci. Technol. B* **28**, C2C9 (2010).
- <sup>14</sup>P. Vincent, S. T. Purcell, C. Journet, and V. T. Binh, *Phys. Rev. B* **66**, 075406 (2002).
- <sup>15</sup>Z. L. Wang, R. P. Gao, W. A. de Heer, and P. Poncharal, *Appl. Phys. Lett.* **80**, 856 (2002).